ACES Asian Chemical Editorial Society

doi.org/10.1002/cnma.202100455

CHEMNANOMAT
Research Article

www.chemnanomat.org

Special Collection

Spherical Polyelectrolyte Brushes Templated Hollow C@MnO Nanospheres as Sulfur Host Materials for Li–S Batteries

Dongjiu Xie,[a, b] Oumeima Jouini,[a, b] Shilin Mei,*[a] Ting Quan,[a] Yaolin Xu,[a] Zdravko Kochovski,[a] and Yan Lu*[a, b]

Abstract: Li–S battery has been considered as the next-generation energy storage device, which still suffers from the shuttle effect of lithium polysulfides (LiPSs). In this work, mesoporous hollow carbon-coated MnO nanospheres (C@MnO) have been designed and synthesized using spherical polyelectrolyte brushes (SPB) as template, $KMnO_4$ as MnO precursor, and polydopamine as carbon source to improve the electrochemical performance of Li–S battery. The hollow C@MnO nanospheres enable the combination of physical confinement and chemical adsorption of the LiPSs. The thin carbon coating layer can provide good electrical conductivity and additional physical confinement to polysulfides. Moreover, the encapsulated MnO inside the carbon shell exhibits strong chemical adsorption to polysulfides. The constructed C@MnO/S cathode shows the discharge capacity of 1026 mAh g^{-1} at 0.1 C with 79% capacity retention after 80 cycles. The synthesized hollow C@MnO nanoparticles can work as highly efficient sulfur host materials, providing an effective solution to suppress the shuttle effect in Li–S battery.

Introduction

Lithium-sulfur (Li–S) batteries are perceived as one of the most promising energy storage devices since they provide the best combination of high capacity, low cost and abundant nature.[1] Importantly, the active material in Li–S battery is capable to reversibly incorporate two electrons per sulfur atom in the conversion redox reaction of sulfur species, while in the insertion-oxide cathodes only one or less than one electron per transition-metal ion can be incorporated.[2] Moreover, Li–S batteries present an outstanding theoretical specific capacity (1675 mAh g^{-1}) as well as high energy density (2600 Wh Kg^{-1}) in comparison with other rechargeable systems.[3] However, several challenges are still to be taken under consideration such as the intrinsic insulating property of sulfur, the formation of Li dendrites, the low active mass loading, the volume expansion of sulfur in the cell (~80%) during the conversion reaction, and the shuttle effect resulted from the dissolution of the intermediate LiPSs formed during the conversion reaction.[4] Many attempts have been made in recent years such as the development of efficient electrolytes, novel electrode materials, and innovative cell configurations to improve the capacity and cycling stability of Li–S battery for the technical and industrial applications.[5]

To efficiently suppress the LiPSs shuttle effect, two main strategies have been reported in the exploration of sulfur host materials. The first strategy is to incorporate sulfur species into nonpolar carbon host materials, including mesoporous or microporous carbon, hollow carbon spheres, and graphene.[6] The introduction of carbon hosts could effectively improve the issue of volume expansion and poor electrical conductivity of sulfur species during the cycling since a certain free space is provided to prevent the electrode deformation. However, the polar LiPSs species could be hardly prevented from dissolving and diffusing into the electrolyte by the physical confinement of carbon, causing severe capacity degradation of Li–S battery due to the weak interaction between the non-polar surface of carbon host and the polar polysulfides.[7] Thus, porous carbon-based materials are inefficient as sulfur host materials without modification or combination with other active component.

Different from carbon-based materials, polar metal-based compounds show a strong chemical interaction with the polysulfides regarding their intrinsic polarity.[8] Among them, metal oxides have been intensively studied as electrode materials in Li–S batteries due to their low cost, non-toxicity, natural abundance and chemical stability.[9] For example, Cui et al. have quantitatively investigated the polysulfide adsorption capability of different polar metal compounds such as metal nitrides, metal oxides, and metal sulfides, finding that manganese oxide exhibits the strongest adsorption ability to LiPSs.[10] However, the low electrical conductivity of metal oxides results in a large charge resistance and fast capacity fading during cycling. Besides, metal oxides exhibit lower specific surface area

[a] D. Xie, O. Jouini, Dr. S. Mei, Dr. T. Quan, Dr. Y. Xu, Dr. Z. Kochovski, Prof. Y. Lu
Department for Electrochemical Energy Storage
Helmholtz-Zentrum Berlin für Materialien und Energie
Hahn-Meitner Platz 1, 14109 Berlin (Germany)
E-mail: yan.lu@helmholtz-berlin.de
meishilina@163.com

[b] D. Xie, O. Jouini, Prof. Y. Lu
Institute of Chemistry
University of Potsdam
Karl-Liebknecht-Straße 24–25, 14476 Potsdam (Germany)

Supporting information for this article is available on the WWW under https://doi.org/10.1002/cnma.202100455

Special Collection *This manuscript is part of a special collection highlighting Asian Women in Materials Chemistry and Nanoscience. Click here to visit the special collections page of the journal.*

compared to carbon-based materials, offering limited spaces or voids for sulfur accommodation.[11] Therefore, combining metal oxides and carbon materials in a multi-functional composite is proposed as an effective approach to develop cathodes with improved conductivity and adsorption ability to improve the performance of Li–S batteries.[12]

Among metal oxides, manganese monoxide has been extensively studied as electrode material in Li ion batteries, sodium-ion batteries, Li-O_2 batteries and zinc-air batteries.[13] Besides, MnO-based materials have attracted increasing attention as sulfur host materials for Li–S batteries.[14] Recently, it has been demonstrated that MnO has great potential to hinder the shuttle effect because of its excellent adsorption capability to polysulfides.[9,15] Besides, the presence of MnO nanoparticles allows the reducing of the nucleation energy for the formation of Li_2S and the acceleration of the phase transformation of solid Li_2S from liquid polysulfides, which enables an efficient conversion and delivers fast kinetics of polysulfide redox reactions.[16] Also, it was reported that the MnO nanoparticles could be embedded into carbon nanofiber by electrospinning method to suppress the shuttle effect of polysulfides.[16–17] Due to the less of voids and pores for sulfur accommodation in these materials, they was insufficient as sulfur host materials, showing limited improvement of electrochemical performance. To achieve high specific surface area, it is favorable to design porous/hollow structure embedded with small MnO nanoparticles. Templating methods have been widely used to create hollow or porous structures for achieving high sulfur loading and polysulfides confinement at the same time.[18] For example, Lin et al. reported that carbon/MnO coaxial nanotubes were successfully synthesized by using MnO_2 nanowire as the template, delivering a specific capacity of 802 $mAh \cdot g^{-1}$ at 5 C with outstanding cycling stability.[19] However, it is a time-consuming process to remove or etching the inorganic template off. With this regard, using spherical polymer brushes as template is a good choice since the polymer template can be completely removed during the calcination process, leading to porous/hollow-structured metal oxide. Moreover, it can easily complex with inorganic precursors by electrostatic interactions, and efficiently stabilize the inorganic nanoparticles to avoid aggregation.

In this work, hollow carbon-coated MnO nanospheres (C@MnO) are synthesized by using spherical polyelectrolyte brushes (SPB) as template, $KMnO_4$ as precursor of MnO and polydopamine (PDA) as carbon source as shown in Scheme 1. Firstly, MnO_4^- ions are introduced into SPB particles by ion exchange process. A thin PDA layer is then coated on the MnO_4^--SPB particles. Finally, the MnO_4^- ions are reduced to MnO nanoparticles, which are embedded into hollow carbon nanospheres after the calcination under argon. The obtained hollow C@MnO nanospheres can provide large space for sulfur loading, volume expansion of sulfur, and physical confinement of polysulfides. Besides, the carbon coating layer enables a good conductivity of the cathode, while the MnO nanoparticles embedded in the carbon can work as chemical adsorber and mediator for LiPSs. Owing to these merits, the constructed C@MnO/S cathode exhibits better electrochemical performance than that of the Carbon/S cathode.

Results and Discussion

The SPB particles contains PS as core, onto which long chains of poly(2-trimethylammoniumethylmethacrylate chloride) brushes have been grafted. To investigate the morphology of the synthesized SPB particles, normal transmission electron microscopy (TEM) have been performed for the dried sample as shown in Figure S1. The particles detain a spherical shape and

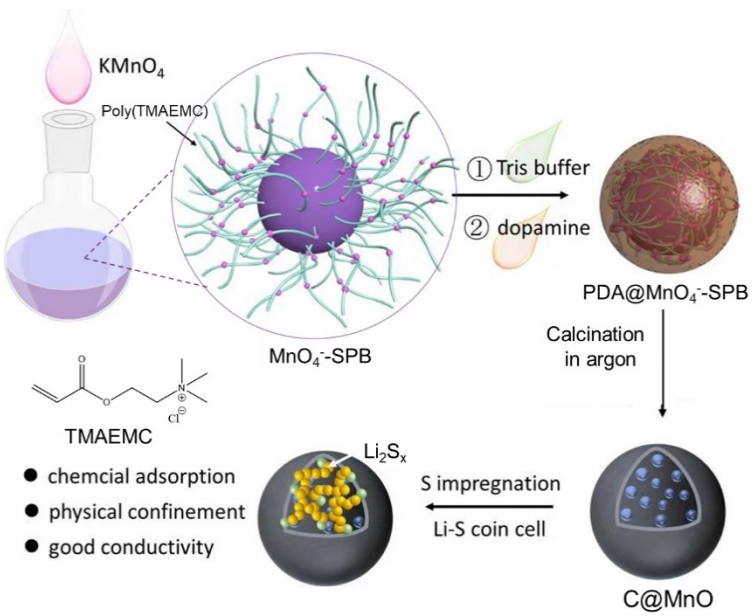

Scheme 1. Schematic synthesis route of the hollow C@MnO nanospheres, which has been used as sulfur host materials for Li–S battery.

uniform size distribution ($\bar{d}$ = 80 nm) in the collapsed state. The particles are not totally separated from each other, which is due to the drying process during the preparation for TEM characterization, where the particles tend to aggregate when the water evaporates, resulting in the connection of the polymer brushes. Figure 1a shows the cryo-TEM image of the SPB nanoparticles, which are well-dispersed and present their native state in the aqueous solution. The polymer brushes are invisible due to the low contrast of the polymer chains in the unstained state.[20] The synthesized SPB particles are positively charged due to the amino groups (–NR^+) from the polymer brushes. As reported by Polzer et al., the MnO_4^- ions can be adsorbed within the SPB brushes via counter ion exchange[21] The maximal capacity of SPB to adsorb MnO_4^- was determined by the potentiometric titration method using $AgNO_3$ solution (20 mM), as shown in Figure S2. It is revealed that after adding 13.8 mL $AgNO_3$ solution into the SPB solution (0.0234 g mL^{-1}), the conductivity of the solution reaches the lowest value, suggesting that 13.8 mM is the maximum concentration of SPB for the adsorption of permanganate ions. In our experiments, excess of $KMnO_4$ was applied to ensure the full complexation of MnO_4^- within the SPB particles. After the addition of $KMnO_4$, the obtained MnO_4^--SPB particles present purple color and the dark contrast on the surface of SPB particles was detected in the TEM image (Figure 1b), indicating the successful ion adsorption.[21a] After dispersing the MnO_4^--SPB particles into the tris-buffer solution (pH = 8.5), the color of particles changes from purple to brown because under weak alkaline condition the MnO_4^- ions can be reduced to MnO_2 by the amino groups of the polymer brushes. Adding dopamine monomer into the solution leads the color change into dark gray, indicating the polymerization of polydopamine. Compared to the pure SPB particles, the surface of the PDA@MnO_4^--SPB particles turns rough (Figure 1c), which is resulted from the PDA coating. No secondary particles can be detected in the TEM image.

The obtained PDA@MnO_4^--SPB particles have been calcinated under argon at 800 °C for 2 h, which results in the hollow spherical structure (Figure 1d and e). The hollow void exhibits the size of 40–50 nm, which is consistent with that of PS core. In addition, small manganese oxide nanoparticles with size of 3–6 nm are found inside the hollow carbon nanospheres, indicating the PDA layer can efficiently prevent the aggregation of the MnO particles during calcination. The XRD patterns in Figure 1f are well matched with the pattern of the MnO phase (PDF 00–001-1206). The five peaks at 35.0°, 40,6°, 58.7°, 70.3° and 73.9° can be assigned to the (111), (200), (220), (311) and (222) planes of the cubic MnO phase, respectively. Thermogravimetric analysis (TGA) measurement under air has been conducted. The content of MnO in the composite is around 14.4 wt.%, which is calculated from the MnO_2 residual based on the TGA result (Figure S3). Without PDA coating, only bulk MnO particles with size of 200–300 nm (Figure S4) are obtained after calcination. No hollow structure has been formed in this case. These particles have been used as comparison for the adsorption ability test to LiPSs. This demonstrates that PDA coating is crucial for constructing the hollow structure and suppressing the growth of the MnO nanoparticles into aggregates. In addition, hollow carbon spheres (Figure S5) have

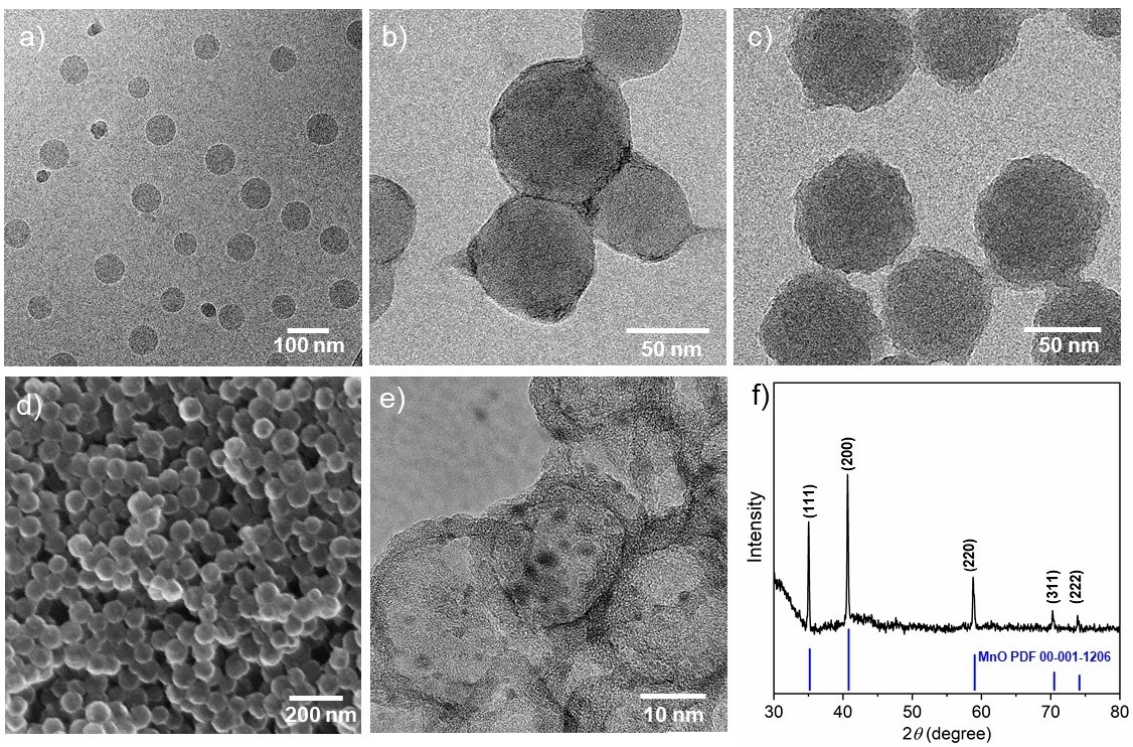

Figure 1. Cryo-TEM image of the SPB particles (a), TEM images of the MnO_4^--SPB particles (b) and PDA@MnO_4^--SPB (c); SEM (d), TEM image (e), and XRD patterns (f) of the hollow C@MnO nanospheres.

been synthesized under the same condition without the presence of $KMnO_4$ to investigate the effects of MnO particles on the electrochemical performance of Li–S battery.

Hollow/porous structures can offer space for high sulfur accommodation and physical confinement for suppressing the shuttle effect of LiPSs. The porous structures of the C@MnO nanospheres have been studied by nitrogen adsorption-desorption measurements. As shown in Figure 2a, a hysteresis loop with a typical IV type isotherm can be observed, suggesting a mesoporous structure[22] of the particles. In Figure 2b, the pore size distribution was further evaluated by using the Barrett-Joyner-Halend (BJH) model.[23] The Brunauer-Emmett-Teller (BET) specific surface area for the C@MnO particles is 192.3 $m^2 g^{-1}$, with pore diameter centered at 6–7 nm. The pure hollow carbon nanospheres possess BET specific surface area of 285.5 $m^2 g^{-1}$ with mesopore size centered at 15 nm. Compared with hollow carbon nanospheres, the smaller mesopores in the C@MnO nanoparticles could exhibit a stronger adsorption capability to LiPSs than that of the larger ones due to its stronger capillary force.[24]

To study the adsorption capacity of the C@MnO nanoparticles to LiPSs (Li_2S_x, $2 < x \leq 8$), a visualized adsorption measurement is performed by adding the same amount of particles (20 mg) in the Li_2S_8 solution (2 mM) solution. The LiPSs solution shows yellow color with the absorption in the wavelength range of 400–500 nm in the UV-*vis* absorption spectra. After adsorption for overnight, it is found that the color of the solution with the C@MnO particles becomes colorless, while the solutions containing bulk MnO and hollow carbon nanospheres powders are only slightly discolored as shown in Figure 2c. The hollow carbon spheres adsorb more polysulfides than bulk MnO particles based on the same mass which is mainly due to its higher specific surface area. This results agree well with the UV-vis absorption spectra (Figure 2d), where the MnO and hollow carbon particles show lower absorption intensity compared to the original LiPSs solution, while the absorption peak of the polysulfides in the wavelength of 400–500 nm diminished for the C@MnO particles owing to the combination of the chemical adsorption of MnO and the physical confinement of the hollow and porous structure. These merits of the C@MnO nanospheres are expected to significantly suppress the shuttle effect of LiPSs.

The electrochemical performance of the hollow C@MnO particles in the Li–S batteries has been investigated in the coin cell form. Sulfur loading in the host nanoparticles has been conducted by the melting diffusion method. The sulfur contents of 58.4% and 58.6% have been determined by TGA for the

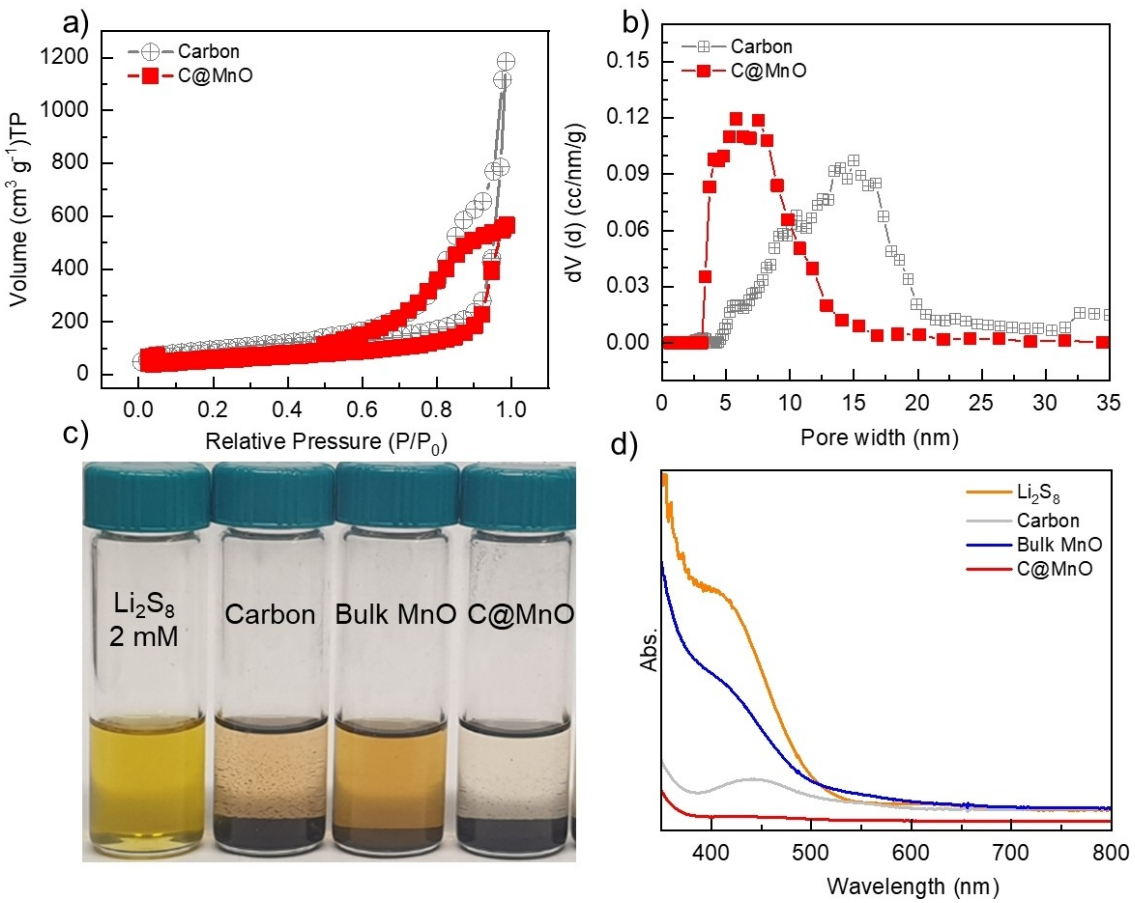

Figure 2. Nitrogen adsorption-desorption isotherms (a) and the pore size distribution curves (b) of the C@MnO (red) and hollow carbon nanospheres (gray); Photograph (c) of a 2 mM Li_2S_8 solution (3 mL) after the addition of hollow carbon, bulk MnO and C@MnO particles (20 mg) for 24 h and the UV-*vis* absorption spectra (d) of the corresponding supernatant solutions.

C@MnO/S and Carbon/S, respectively (Figure S6). Figure 3a presents the CV curves of the coin cell batteries with C@MnO/S cathodes between 1.8 and 3.0 V (*vs.* Li/Li^+) with a scan rate of 0.1 $mV\,s^{-1}$. The initial cathodic scan shows two reduction peaks at 2.3 and 2.0 V, corresponding to the conversion of sulfur to long-chain LiPSs (Li_2S_n, $4 \leq n \leq 8$) and further to short-chain lithium sulfide (Li_2S_2/Li_2S), respectively. In the anodic scan, the two peaks at 2.3 and 2.4 V are assigned to the oxidation process of Li_2S to short-chain LiPSs intermediates and then to sulfur, respectively.[25] In the subsequent cycles, good overlapping of the CV curves can be observed, indicating a stable charging-discharging process. Figure 3b shows the galvanostatic charge-discharge profiles of the Li–S batteries with C@MnO/S and Carbon/S as cathode at 0.1 C. In both cases, one charge plateau and two typical discharge plateaus are clearly shown in Figure 3b, which agrees with the CV curves. In addition, the C@MnO/S cathode exhibits a slightly lower overpotential than that of the Carbon/S one due to its lower impedance value (Figure S7). As shown in the electrochemical impedance spectroscopy (EIS) plot, the *Rct* of the Li–S cell with C@MnO/S cathode is 83 Ω while that of Carbon/S is 223 Ω.

Figure 3c presents the cycling performance of different Li–S cells at 0.1 C for 80 cycles. The Carbon/S cathode delivers an initial discharge capacity of 870 $mAh\,g^{-1}$, which drops to

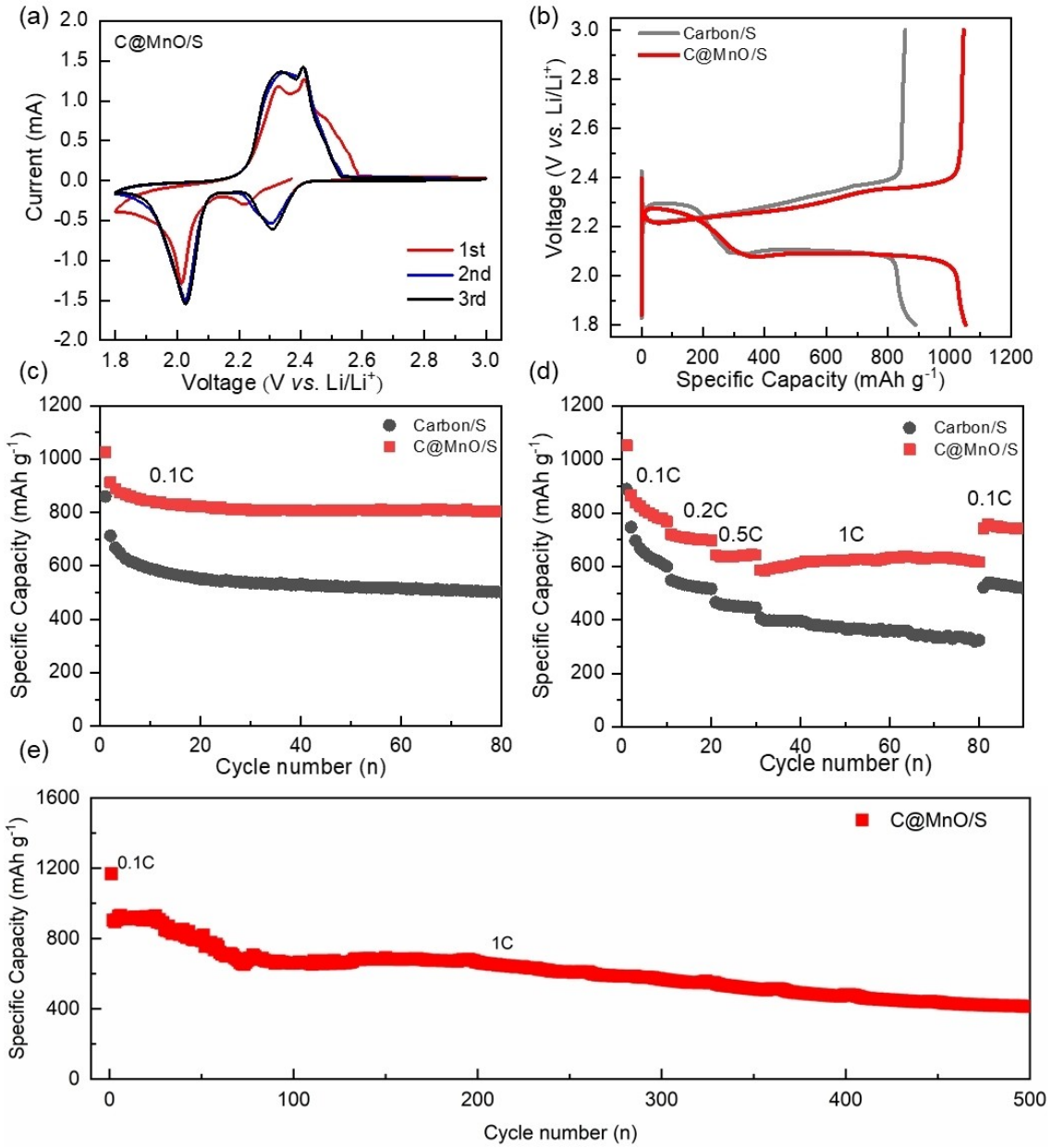

Figure 3. CV profiles of the Li–S coin cell with C@MnO/S as cathode (a), the charge-discharge curves (b), cycling performance (c), and rate capacity (d) of the Li–S coin cell with C@MnO/S and Carbon/S as cathode, respectively; the long-term cycling performance (e) of the Li–S cell with the C@MnO/S as cathode at 1 C (1 C = 1675 $mA\,g^{-1}$). The areal loading of sulfur is around 2 $mg\,cm^{-2}$ in the cathode.

500 mAh g^{-1} after 80 cycles with the capacity retention of 57.5%. In contrast, C@MnO/S cathode delivers a much higher initial discharge capacity of 1026 mAh g^{-1}. After 80 cycles, the discharge capacity remains at 820 mAh g^{-1} corresponding to the capacity retention of 79.9%. The better cycling performance of the C@MnO/S cathode reveals the crucial role of the MnO nanoparticles, which can suppress the LiPSs dissolution by chemical adsorption. The polar O–Mn–O units in MnO have strong affinity to polysulfides via chemical interaction and inhibit their diffusion through the electrolyte to the anode side of the battery.[16] The rate capabilities have been further measured by increasing the applied current density from 0.1 C to 1 C and then reducing to 0.1 C, as presented in Figure 3d. The discharge capacities of the C@MnO/S cathodes are initially 700, 642, and 586 mAh g^{-1} at 0.2, 0.5, and 1 C, respectively, while the Carbon/S cathode only delivers 548, 465, 406 mAh g^{-1} at 0.2, 0.5, and 1 C, respectively. The C@MnO/S cathodes show better rate capability when compared to that of the Carbon/S electrode especially at high current rate of 1 C. Higher discharge capacities of 550–600 mAh g^{-1} at 1 C are delivered by the C@MnO cathodes, while only 400 mAh g^{-1} has been obtained by the Carbon/S cathode. This difference can be explained by the strong capability of MnO to adsorb polysulfides, which is beneficial for a fast-redox reaction on the catalytic surface of the metal oxide hosts.[15b] When it returns to 0.1 C, the discharge capacity is recovered to 790 mAh g^{-1} and 550 mAh g^{-1} for C@MnO/S and Carbon/S, respectively. This suggests a good reversibility of the sulfur redox reaction under different current rates. The cycling stability of the coin cell batteries with C@MnO/S as cathode has been measured at 1 C. It delivers a discharge capacity of 412 mAh g^{-1} after 500 cycles with the capacity fading of 0.1% per cycle. The improved electrochemical performance of the C@MnO particles is due to the following advantages: firstly, the MnO nanoparticles serve as chemical adsorber and mediator for LiPSs; secondly, the hollow structure can provide large space for tolerating the volume expansion of lithiated sulfur and offer physical confinement of polysulfides; thirdly, the carbon coating layer enables a good conductivity of the cathode. In addition, the synthesis approach of the C@MnO particles can be up-scaled, which is essential for the potential application of commercialized Li–S battery in future.

Conclusion

In this work, C@MnO hollow nanospheres have been designed and synthesized using spherical polyelectrolyte brushes (SPB) as template, $KMnO_4$ as MnO precursor, and polydopamine (PDA) as the carbon source. The obtained C@MnO nanoparticles show a high specific surface area of 192.3 m^2 g^{-1} with mesopores of 6–7 nm. The constructed C@MnO/S cathode shows a higher discharge capacity of 1026 mAh g^{-1} at 0.1 C compared to that of Carbon/S cathode and delivers better rate capability at 1 C with a capacity of 586 mAh g^{-1}. This is due to the fact that MnO with the polar surface provides a strong chemical adsorption to LiPSs and inhibits their dissolution in liquid electrolyte. Meanwhile, the hollow/porous carbon layer improves the electrical conductivity and gives additional physical confinement to polysulfides. Such C@MnO/S cathode shows higher specific capacity and rate performance than that of Carbon/S electrode even with a small amount of MnO loading, revealing the crucial role of MnO in improving the electrochemical performance.

Experimental Section

Chemicals

1-[4-(2-Hydroxyethoxy)-phenyl]-2-hydroxy-2-methyl-1-propanone (Irgacure 2595, Ciba), pyridine (Fluka), methacryloyl chloride (MC, Fluka), cetyltrimethylammonium bromide (CTAB, Fluka), 2,2′-azobis(2-amidinopropane)dihydrochloride (V50, Wako), Tris (Roth), divinylbenzene (DVB, Merck) were used as received. 2-trimethylammoniumethylmethacrylate chloride (TMAEMC), potassium permanganate ($KMnO_4$), carbon disulfide (CS2), silver nitrate ($AgNO_3$,), N-methylpyrrolidinone (NMP), 1, 3-dioxolane (DOL), polyvinylidene fluoride (PVDF), 1, 2-dimethoxyethane (DME) and sodium borohydride ($NaBH_4$) were purchased from Sigma-Aldrich and used directly. The inhibitor (4-tert-butylcatechol) in the styrene (Sigma-Aldrich) must be first removed by inhibitor remover (Sigma-Aldrich) via column and then the styrene can be stored in the fridge at 4 °C before use. 2-[p-(2-Hydroxy-2-methylpropiophenone)]-ethylene glycol methacrylate (HMEM) was applied as the photo-initiator for grafting of the brushes onto the polystyrene (PS) cores. All the solvents are used as received. The used deionized water ($\kappa \leq 0.05$ μS cm^{-1}) is purified by ion exchange (Millipore Milli-Q) system.

Synthesis of template: spherical polyelectrolyte brushes (SPB)

The synthesis of cationic SPB lattices is performed under a three-step process according to the previous work of Guo et al.[26] Firstly, polystyrene (PS) particles are synthesized using the emulsion polymerization method. A thin layer of photo-initiator HMEM is coated on the surface of the PS cores via injection during the polymerization. Finally, the photo-initiated polymerization of the monomer TMAEMC (grafting on technique) is conducted under UV light irradiation to induce the growth of polymer brush on the surface of PS core.

Titration to determine the Cl^- ion concentration in SPB

10 mL of SPB solution (0.0234 g mL^{-1}) is diluted by adding 10 mL H_2O under stirring (250 rpm). A certain amount of $AgNO_3$ solution (20 mM) is then added to the SPB solution and the conductivity is measured continuously using the WTW cond 197i conductometer. By adding the $AgNO_3$ solution, Ag^+ cations form AgCl precipitate with Cl^- anions and the solution becomes turbulent. As a result, the conductivity of the solution tends to drop at first as the Cl^- ions are consumed. After the titration point is reached, the conductivity increases again since the solution contains an excess of Ag^+ cations.

Synthesis of hollow C@MnO and hollow carbon nanospheres

In a typical run, 20 mL of SPB solution (solid content 0.0234 g mL^{-1}) and $KMnO_4$ solution (0.468 g dissolved in 20 mL H_2O) are treated separately with N_2 for at least 20 min for degassing. After slowly adding $KMnO_4$ drop by drop into the SPB solution, the N_2 flow is kept for 15 min. Then, the solution is kept under stirring overnight. The particles are collected by centrifugation under the speed of

8000 rpm for 20 min for the removal of the exceeding non-adsorbed salts then wash it with water for three times. The collected particles are then dispersed into 50 mL of tris-buffer solution (pH = 8.5). After 15 mins' stirring in an ice bath, a color change can be observed (from purple to brown). After 30 min, 2.34 g of dopamine hydrochloride dissolved in water (5 mL) is added to the solution. The ice-bath is kept for additional 3 h to slow down the polymerization process to obtain a uniform PDA layer coated on the MnO_4^--SPB particles. After stirring overnight at room temperature, the sample is cleaned via ultrafiltration using a 50 nm pores size cellulose nitrate filters. In the end, the collected product is annealed in argon at 800 °C for 2 h with a ramping rate of 3 °C min^{-1}. The synthesis of the hollow carbon nanospheres is via coating of PDA on the surface of the SPB nanoparticles without $KMnO_4$ in the solution, which is similar with that of the C@MnO nanoparticles.

Synthesis of the bulk MnO particles

Firstly, 20 mL of SPB solution (0.0234 g mL^{-1}) and $KMnO_4$ solution (0.468 g dissolved in 20 mL H_2O) are treated separately with N_2 for at least 20 min for degassing. After slowly adding $KMnO_4$ drop by drop into the SPB solution, the mixture is stirring for overnight under N_2. Then, 0.11 g of $NaBH_4$ solution (5 mL) is added into the solution. The mixture is centrifuged after stirring for 30 min and re-dispersed into water for three times. Followed the calcination at 800 °C for 2 h under argon, the bulk MnO particles are obtained.

Synthesis of the C@MnO/S composite

C@MnO nanoparticles and sulfur are mixed at a mass ratio of 2:3 in 1 mL CS_2 and kept in the fume hood for drying. The obtained C@MnO/S composites are further dried at 50 °C for 1 h in the oven. Subsequently, the mixture is heated at 155 °C for at 12 h in a sealed vessel.

Li_2S_8 adsorption capability test

Li_2S_8 solution is prepared via the reaction of S and Li_2S with a fixed molar ratio of 7:1 in the DOL/DME solution (volume ratio 1:1), which is stirred at 80 °C for 48 h in the Ar-filled glove box. 20 mg of host material (C@MnO, hollow C and MnO) powders are added into the Li_2S_8 solution (2 mM, 3 mL), respectively. After keeping in the glove box for 12 h, the supernatant liquid is collected for UV-*vis* spectroscopy test in a sealed cylinder quartz. The hollow carbon and pure MnO powders are used as reference.

Electrochemical testing

The cathodes are prepared via mixing the synthesized C@MnO composite, PVDF binder and Super P powder with a mass ratio of 8:1:1 in NMP solution to generate a homogeneous slurry. The mixture is then spread onto carbon coated aluminium foil using a doctor blade and dried in a vacuum oven at 50 °C for 24 h. To form a coin shaped electrode, the dried foil sheets are pressed to form a densely film and cut into circular disks (d = 9.5 mm). The areal mass loading of sulfur is ~2 mg cm^{-2}. The cathode is then assembled into CR2032-type coin cells using Li metal chip as anode, 40 μL of 1 M LiFTSI solution with 0.2 M $LiNO_3$ in DOL and DME (volume ratio of 1:1) as electrolyte, and Celgard film as separator. The coin cells are Galvano-statically cycled between 1.8 and 3.0 V vs. Li/Li^+ at different C rates (1 C = 1675 mA g^{-1}) with a battery testing system (NEWARE, China). The CV is recorded within a voltage window of 1.8–3.0 V *vs.* Li/Li^+ at a scan rate of 0.1 mV s^{-1} on multi-channel potentiostat (Bio-logic Science) system. The electrochemical impedance spectroscopy (EIS) is measured with the frequency range of 10^5-10^{-2} Hz and a disturbance amplitude of 10 mV on GAMRY Interface 1000. The specific capacity is calculated from the S mass per cathode.

Material characterizations

The morphology of the C@MnO nanospheres is studied by a LEO 1530 field emission scanning electron microscope (SEM). Transmission electron microscopy (TEM) images are obtained using a JEOL JEM-2100 instrument. The acceleration voltage applied is 200 kV. XRD measurements are conducted using a Bruker D8 diffractometer with Cu Kα radiation. N_2 adsorption/desorption isotherms are performed with the Quantachrome Autosorb-1 systems at 77 K. The specific surface areas of the C@MnO particles are calculated by the Brunauer-Emmett-Teller (BET) method on the basis of the multipoint analysis. UV-*vis* spectra (300–800 nm) are measured by using Lambda 650 spectrometer (Perkin-Elmer) at 20 °C. Cryo-TEM specimens were vitrified by plunging the samples into liquid ethane using an automated plunge freezer (Vitrobot Mark IV, FEI). Approximately 5 μL of a pre-heated 0.025 wt.% solution were deposited on the lacey carbon copper grid (200 meshes, Science Services) and equilibrated at the adjusted temperature for 2 minutes in a water-saturated atmosphere. After blotting the liquid, the specimens were vitrified, inserted into a pre-cooled Gatan 914 sample holder and transferred into a JEOL JEM-2100, operating at 200 kV. Thermogravimetric analysis is carried out on PerkinElmer (TGA 8000) in the temperature range of 30–900 °C at a heating rate of 10 °C min^{-1} under N_2 for sulfur content or air for MnO content.

Acknowledgements

The authors thank Dr. Eneli Monerjan at Helmholtz-Zentrum Berlin for the TGA measurement. The authors also thank the Joint Lab for Structural Research at the Integrative Research Institute for the Sciences (IRIS Adlershof). Open Access funding enabled and organized by Projekt DEAL.

Conflict of Interest

The authors declare no conflict of interest.

Data Availability Statement

The data that support the findings of this study are available from the corresponding author upon reasonable request.

Keywords: hollow nanospheres · lithium-sulfur battery · manganese monoxide · sperical polyelectrolyte brushes

[1] S. Dörfler, H. Althues, P. Härtel, T. Abendroth, B. Schumm, S. Kaskel, *Joule* **2020**, *4*, 539–554.
[2] P. Adelhelm, P. Hartmann, C. L. Bender, M. Busche, C. Eufinger, J. Janek, *Beilstein J. Nanotechnol.* **2015**, *6*, 1016–1055.
[3] A. Manthiram, S. H. Chung, C. Zu, *Adv. Mater.* **2015**, *27*, 1980–2006.

[4] a) D. Liu, C. Zhang, G. Zhou, W. Lv, G. Ling, L. Zhi, Q. H. Yang, *Adv. Sci.* **2018**, *5*, 1700270; b) Y. X. Yin, S. Xin, Y. G. Guo, L. J. Wan, *Angew. Chem. Int. Ed.* **2013**, *52*, 13186–13200; *Angew. Chem.* **2013**, *125*, 13426–13441.
[5] a) Y. T. Liu, S. Liu, G. R. Li, X. P. Gao, *Adv. Mater.* **2021**, *33*, 2003955; b) S. Li, Z. Fan, *Energy Storage Mater.* **2021**, *34*, 107–127; c) L. Chen, H. Yu, W. Li, M. Dirican, Y. Liu, X. Zhang, *J. Mater. Chem. A* **2020**, *8*, 10709–10735; d) W. Chen, T. Lei, C. Wu, M. Deng, C. Gong, K. Hu, Y. Ma, L. Dai, W. Lv, W. He, X. Liu, J. Xiong, C. Yan, *Adv. Energy Mater.* **2018**, *8*, 1702348.
[6] a) X. Ji, K. T. Lee, L. F. Nazar, *Nat. Mater.* **2009**, *8*, 500–506; b) G. He, S. Evers, X. Liang, M. Cuisinier, A. Garsuch, L. F. Nazar, *ACS Nano* **2013**, *7*, 10920–10930; c) N. Jayaprakash, J. Shen, S. S. Moganty, A. Corona, L. A. Archer, *Angew. Chem. Int. Ed.* **2011**, *50*, 5904–5908; d) Q. Zhao, T. P. Fellinger, M. Antonietti, J. Yuan, *J. Mater. Chem. A* **2013**, *1*, 5113–5120.
[7] X. Tao, J. Wang, C. Liu, H. Wang, H. Yao, G. Zheng, Z. W. Seh, Q. Cai, W. Li, G. Zhou, C. Zu, Y. Cui, *Nat. Commun.* **2016**, *7*, 11203.
[8] a) H. Wang, W. Zhang, J. Xu, Z. Guo, *Adv. Funct. Mater.* **2018**, *28*, 1707520; b) S. Saeedi Garakani, D. Xie, A. K. Kheirabad, Y. Lu, J. Yuan, *Mater. Adv.* **2021**, *2*, 5203–5212; c) D. Xie, S. Mei, Y. Xu, T. Quan, E. Härk, Z. Kochovski, Y. Lu, *ChemSusChem* **2021**, *14*, 1404.
[9] K. Liao, H. Wei, P. Shi, J. Fan, Q. Xu, Y. Min, *J. Mater. Chem. A* **2020**, *8*, 21163–21172.
[10] D. S. Wu, F. Shi, G. Zhou, C. Zu, C. Liu, K. Liu, Y. Liu, J. Wang, Y. Peng, Y. Cui, *Energy Storage Mater.* **2018**, *13*, 241–246.
[11] L. Borchardt, M. Oschatz, S. Kaskel, *Chem. Eur. J.* **2016**, *22*, 7324–7351.
[12] Z. Li, H. B. Wu, X. W. Lou, *Energy Environ. Sci.* **2016**, *9*, 3061–3070.
[13] L. Chen, X. Guo, W. Lu, M. Chen, Q. Li, H. Xue, H. Pang, *Coord. Chem. Rev.* **2018**, *368*, 13–34.
[14] a) Y. Feng, H. Liu, Q. Lu, Y. Liu, J. Li, X. He, X. Liu, D. Mikhailova, *J. Power Sources* **2022**, *520*, 230885; b) W. Liu, X. Fan, B. Xu, P. Chen, D. Tang, F. Meng, R. Zhou, J. Liu, *Nano Select* **2021**, *2*, 573–580; c) M. Xiang, H. Zhang, S. Feng, J. Xiao, X. Li, *J. Electroanal. Chem.* **2021**, *900*, 115721; d) P. Qiu, Y. Yao, W. Li, Y. Sun, Z. Jiang, B. Mei, L. Gu, Q. Zhang, T. Shang, X. Yu, J. Yang, Y. Fang, G. Zhu, Z. Zhang, X. Zhu, T. Zhao, W. Jiang, Y. Fan, L. Wang, B. Ma, L. Liu, Y. Yu, W. Luo, *Nano Lett.* **2021**, *21*, 700–708.
[15] a) X. Qian, L. Jin, D. Zhao, X. Yang, S. Wang, X. Shen, D. Rao, S. Yao, Y. Zhou, X. Xi, *Electrochim. Acta* **2016**, *192*, 346–356; b) Y. Liu, G. Feng, X. Guo, Z. Wu, Y. Chen, W. Xiang, J. Li, B. Zhong, *J. Alloys Compd.* **2018**, *748*, 100–110.
[16] M. Chen, T. Li, Y. Li, X. Liang, W. Sun, Q. Chen, *ACS Appl. Energ. Mater.* **2020**, *3*, 10793–10801.
[17] J. Zhu, R. Pitcheri, T. Kang, Y. Guo, J. Li, Y. Qiu, *Ceram. Int.* **2018**, *44*, 16837–16843.
[18] A. Fu, C. Wang, F. Pei, J. Cui, X. Fang, N. Zheng, *Small* **2019**, *15*, 1804786.
[19] C. Lin, L. Qu, J. Li, Z. Cai, H. Liu, P. He, X. Xu, L. Mai, *Nano Res.* **2019**, *12*, 205–210.
[20] Y. Lu, M. Ballauff, *Prog. Polym. Sci.* **2016**, *59*, 86–104.
[21] a) F. Polzer, D. A. Kunz, J. Breu, M. Ballauff, *Chem. Mater.* **2010**, *22*, 2916–2922; b) F. Polzer, E. Holub-Krappe, H. Rossner, A. Erko, H. Kirmse, F. Plamper, A. Schmalz, A. H. E. Müller, M. Ballauff, *Colloid Polym. Sci.* **2013**, *291*, 469–481.
[22] G. Pickett, *J. Am. Chem. Soc.* **1945**, *67*, 1958–1962.
[23] E. P. Barrett, L. G. Joyner, P. P. Halenda, *J. Am. Chem. Soc.* **1951**, *73*, 373–380.
[24] W. Zhou, C. Wang, Q. Zhang, H. D. Abruña, Y. He, J. Wang, S. X. Mao, X. Xiao, *Adv. Energy Mater.* **2015**, *5*, 1401752.
[25] a) S. Mei, C. J. Jafta, I. Lauermann, Q. Ran, M. Kärgell, M. Ballauff, Y. Lu, *Adv. Funct. Mater.* **2017**, *27*, 1701176; b) D. Zheng, X. Zhang, J. Wang, D. Qu, X. Yang, D. Qu, *J. Power Sources* **2016**, *301*, 312–316.
[26] X. Guo, A. Weiss, M. Ballauff, *Macromolecules* **1999**, *32*, 6043–6046.

Manuscript received: November 14, 2021
Revised manuscript received: December 21, 2021
Accepted manuscript online: February 10, 2022
Version of record online: March 16, 2022